JETI
Journal of Experimental and Tecnique Instrumentation
UFMS
Review

Experimental charge-density analysis towards predictive materials science

*Camila B. Pinto, Bernardo L. Rodrigues, Leonardo H. R. Dos Santos**

Departamento de Química, Universidade Federal de Minas Gerais, Av. Antônio Carlos 6627, 31270-901 Belo Horizonte MG, Brazil
* e-mail: leonardohrs@ufmg.br

DOI: https://doi.org/10.30609/jeti.v4i3.12820

Abstract. The ongoing increase in the number of experimental charge-density studies can be related to both the technological advancements and the wide applicability of the method. Regarding materials science, the understanding of bonding features and their relation to the physical properties of materials can not only provide means to optimize such properties, but also to predict and design new materials with the desired ones. In this tutorial, we describe the steps for a charge-density analysis, emphasizing the most relevant features and briefly discussing the applications of the method

Keywords: electron distribution, charge distribution, quantum theory of atoms in molecules, molecular materials, X-ray diffraction

1. Introduction

Over the last decade, there has been an increase in the number of crystal structures which are further analyzed in terms of a charge density study, as can be demonstrated through a search on the *Cambridge Structural Database* [1], Fig. 1(a). This follows the prediction of the pioneers of X-ray diffraction in the early 1900's [2] and shows the clear applicability of X-ray radiation in charge density studies. The increase is related to both the potentialities of the technique and the advancements in hardware and software, which have not only allowed more accurate, but also a faster data collection. Charge density studies date back to the 1960s with deformation density studies on organic compounds such as α-oxalic acid dihydrate and S-triazine [3], and while the development of desktop computers has surely contributed to an increase in charge density studies in recent years (by efficiently optimizing highly-parameterized least-squares cycles), technical improvements in data collection hardware also play an important role. The use of low temperature, for

instance, allows the collection of very accurate reflections at higher resolutions, which is essential for a proper deconvolution of the electron density deformation due to thermal motion from that due to chemical bonding. Even though low temperatures down to liquid nitrogen (approximately 100 K) are sufficient for most charge density studies, it has been demonstrated [4] that even lower temperatures, such as that for liquid helium (approximately 10 K), yields better results and also helps avoiding systematic errors. Such extreme temperatures, despite still accounting for the minority of the study temperatures, Fig. 1(b), have become more frequent since 2005 as a consequence of advancements in instrumentation. It is also possible to see that some measurements have been conducted at room temperature. These experiments can be related, for example, to studies intended to compare atomic displacement parameters obtained at different temperatures (*e.g.* [5,6]).

Notwithstanding, the development of area detectors has also represented an improvement in data collection due to the possibility of acquiring accurate data in shorter periods of time, decreasing the time of crystal exposure to radiation, hence the risk of crystal decay or complete degradation. The use of synchrotron radiation, a highly brilliant source, is also worthy to note, since it allows faster and very accurate data acquirement with very small X-ray wavelengths, as well as the use of smaller samples, minimizing absorption and extinction effects [7].

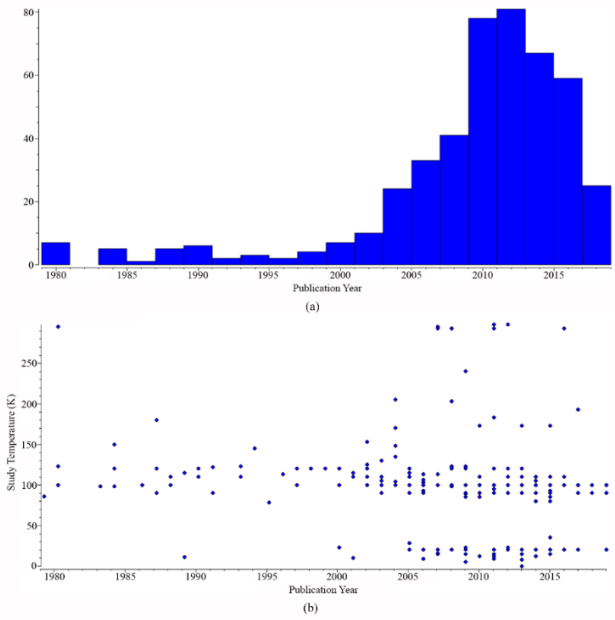

Figure 1. (a) Histogram of structures deposited in CSD (version 5.41) presenting the words "multipole" or "charge density" according to publication year. (b) Scatterplot of structure's publication year *versus* study temperature. The filters used in the search were 3D coordinates determined and only single-crystal structures.

Apart from the abovementioned developments in hardware, improvements in software power and modelling have also contributed to an increase in amount and robustness of charge density studies. For instance, the topological analysis based on the Quantum Theory of Atoms in Molecules [8] allows for a more detailed evaluation of the nature and strength of chemical bonds. In addition, the expansion of calculated wave functions to heavier elements and its implementation in databanks allow for the refinement of molecules containing atoms up to Cf (Z=98) [9]. The combination of all these advancements in the last decades have also increased the applicability of this type of study. Not only it is possible to extract atomic charges or higher electrostatic moments for a molecule or a particular atom or functional group, but it is also possible to correlate charge density parameters to magnetic [10] and optical properties [11], evaluate rearrangements upon application of high pressure [12], or even transfer atomic properties to equivalent atoms in other molecules [13], aiding the prediction and development of new functional materials.

Herein we perform a step-by-step multipole refinement to serve as a tutorial guide for the newcomer to the field. We use an already studied simple organometallic, namely $Cr(CO)_6$, and briefly discuss each refinement stage, emphasizing electron density derived properties and parameters that could be used to help on the rational design of new materials in crystalline form, either organic, metal-organic, organometallic or inorganic. The data for this refinement was taken from Figgis & Sobolev [14], and charge density studies for this molecule have already been conducted by Rees & Mitschler [15] and Farrugia & Evans [16].

2. Data Collection and Quality Assessment

The data collection to perform a charge density analysis presents some particularities in comparison to the data acquisition for a conventional structure determination. Charge density analyses are concerned with the information related to bonding features and interactions, hence the information on valence electrons is necessary. The information on such electrons is restricted to lower angles and usually represent only a small fraction of the total number of electrons, so it is important to measure the reflections at this region with high redundancy and high signal-to-noise ratio. In addition, data should be acquired to high angles, achieving a resolution of $(\sin\theta)/\lambda \geq 1.1$ Å^{-1}. These reflections measured at higher angles will aid the deconvolution of electron deformation due to

chemical bonding from that due to the thermal motion of atoms. The use of low temperature is also crucial to lower the thermal vibration, enhancing the quality of the data collected at higher angles and decreasing systematic errors, since the intensities at these angles tend to be weaker [7,17] .

The evaluation of the collected data quality can be done through a statistical analysis, by evaluating the values of R_{int}, ‹I/σ(I)›, redundancy and completeness *vs.* resolution. Good quality data should present high values of I/σ(I), redundancy and completeness at lower angles, and low values of R_{int} [17]. The results on the multipole refinement will also inform on the data quality, as will be discussed in this tutorial guide.

3. Refinement Steps

The starting point for an aspherical atom refinement, that is, one which takes into account the deformation density related to chemical bonding (as opposed to the more traditional crystal structure determination refinement which considers only spherically averaged, isolated atoms), is to obtain the initial atomic coordinates, meaning that a conventional structural determination needs to be performed *a priori*. This more common step will not be discussed here, but the main results are summarized in the next paragraphs and in Table 1.

The molecule $Cr(CO)_6$ presents an almost ideal octahedral geometry, crystallizing in the *Pnma* space group, with four molecules per unit cell. The measurement was conducted at 11 K, collecting 27649 reflections with 4212 independent observations. Further information regarding data collection can be found in reference [14]. The structure was solved by the Patterson function, through the program SHELXS-86 [18], and positional and thermal parameters were optimized through full-matrix least-squares procedure through SHELXL-2016/6 [19]. Fig. 2 presents the thermal ellipsoid representation of the molecule under study. It presents a mirror plane, so atoms Cr, C(1), C(2), O(1) and O(2) have an occupation of 0.5, as they define the symmetry element, while atoms $C(3)^i$, $C(4)^i$, $O(3)^i$ and $O(4)^i$ are generated through the symmetry operation (i) *x*, ½-*y*, *z*.

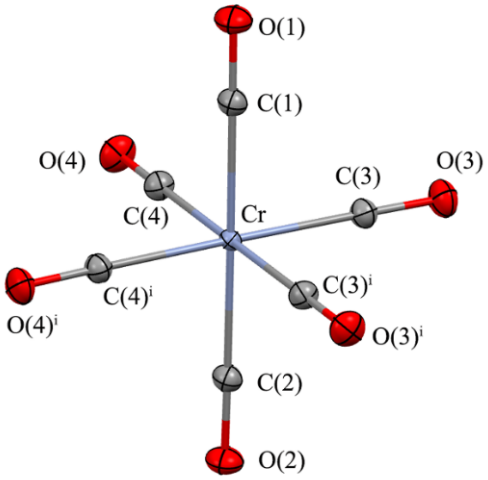

Figure 2. Ellipsoid representation of $Cr(CO)_6$. Ellipsoids drawn at 80% probability level. Symm. op. (i): x, $½-y, z$.

Table 1. Experimental details for $Cr(CO)_6$

Chemical Formula	CrC_6O_6
M_r	220.06
Crystal system, space group	Orthorhombic, *Pnma*
Temperature (K)	11(2)
a, b, c (Å)	11.4740(10), 10.8940(10), 6.1885(4)
V (Å^3)	773.55(11)
Z	4
$\sin(\theta_{max})/\lambda$	1.080
No. of independent reflections	4212
Spherical Atom Refinement	
No. of reflections in the refinement	4212
Refined parameters	68
$R[F^2 > 2\sigma(F^2)]$, $wR(F^2)$, S	0.020, 0.054, 1.158
$\Delta\rho_{max,min}$ (eÅ^{-3})	0.85, -0.99
Multipole Refinement*	
No. of reflections in the refinement	4021
Refined parameters	194
$R[F^2 > 3\sigma(F^2)]$, $wR(F^2)$, S	0.013, 0.016, 1.921
$\Delta\rho_{max,min}$ (eÅ^{-3})	0.22, -0.22

*Performed using the XD2016 program [20]

The conventional structural determination follows the approximation that the atoms are spherical, isolated and in their ground state. This approximation is known as the *Independent Atom Model* (IAM), and can be represented by Eq. (1) [21], where ρ_{ej} is the spherically averaged probability of finding the jth electron in the volume dv.

$$\rho^0_{atom}(\boldsymbol{r})\,dv = \left(\sum_j^Z \rho_{ej}\right) dv \qquad (1)$$

This approximation is sufficient for structural determination and for analyses of molecular geometry and packing arrangements; however, it is not enough for the study of chemical bonds or the extraction of properties, such as dipole moments. The fact that this approach does not take into account deformation density can be readily seen through the residual density maps. These maps plot the difference between the observed structure factors (F_{obs}) and those calculated based on the model (F_{calc}), Eq. (2).

$$\delta\rho^{res}(\boldsymbol{r}) = \frac{1}{V}\sum_{\boldsymbol{h}}[|F_{obs}(\boldsymbol{h})| - |F_{calc}(\boldsymbol{h})|]\exp(i\phi_{calc})\exp(-2\pi i\boldsymbol{h}\cdot\boldsymbol{r}) \quad (2)$$

If the model considers the electron density as spherical, the final residual map will present density accumulation in the regions related to chemical bonds and lone pairs (regions not accounted for in the IAM). The residual density map obtained for $Cr(CO)_6$ after conventional refinement is depicted in Fig. 3(a), where it is possible to see a density accumulation in the regions related to chemical bonds and oxygen lone pairs. In addition, the analysis of the way the residual noises are distributed can be an indicator of data quality. If no systematic errors are present, the residual density will be normally distributed [22]. This evaluation can be performed through a probability distribution plot, as the one displayed in Fig. 3(b). According to the plot, the residual density for the conventional refinement is close to a Gaussian distribution; however, it extends from -0.8 to 0.8 eÅ^{-3}, demonstrating high residual density for this model.

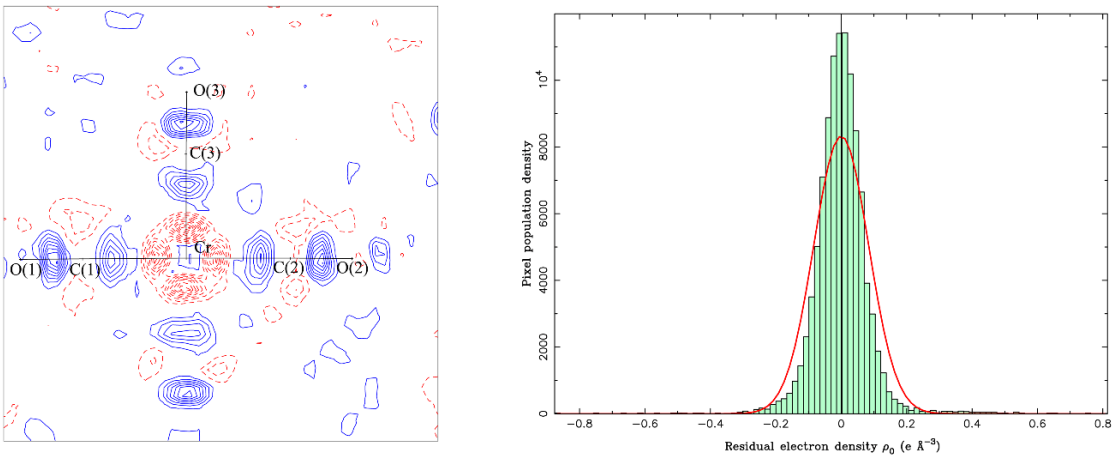

(a) (b)

Figure 3. (a) Residual density map after IAM refinement in the plane Cr–C(2)–C(3) (contours at 0.1 eÅ^{-3}, positive contours are solid blue, negative contours are dashed red). (b) Probability distribution plot for the IAM refinement.

An extension of the IAM, which accounts for the charge transfer between atoms, is known as κ-formalism, and it is usually taken as the next step on the aspherical atom refinement. This formalism still treats the atom as spherical, however, it allows the expansion or contraction of the valence shell due to electron transfer, as a result of chemical bonding. To perform the κ refinement, two parameters need to be simultaneously refined for each atom in the asymmetric unit: P_v (valence population) and κ (the parameter related to the expansion or contraction of the valence shell) [23]. The introduction of these parameters splits the total atomic density into contributions from the electronic core and valence, thus transforming Eq. (1) into Eq. (3):

$$\rho_{atom}(\boldsymbol{r}) = \rho_{core}(\boldsymbol{r}) + P_v \kappa^3 \rho_{valence}(\kappa r) \tag{3}$$

The κ parameter correlates to the atomic charge in an almost linear manner [24], where values of $\kappa > 1$ indicate a contraction of the valence shell, thus a positive charge is for example obtained for a metal, and values of $\kappa < 1$ indicate an expansion of the valence shell, and hence, charges closer to negative values are usually obtained. Since the crystal is neutral, a total charge close to zero is a good indicator of the refinement reasonableness. For the molecule under study, the P_v, κ and atomic charge (q) values obtained after the κ-formalism refinement are listed in Table 2. Through the knowledge of the charges and their distribution in a crystal, it is possible to calculate electric moments, the electrostatic potential and its derivatives [23]. These quantities are strongly related to the intermolecular interactions and the way molecules pack together in a crystal. For instance, a polar molecule will pack in a manner so that the opposite charges are close to each other, and this electrostatic interaction will affect the dipole moments. In addition, the electrostatic potential can be informative, for example, in the study of chemical reactivity, since a nucleophilic reagent tends to be attracted to regions of positive potential whereas electrophilic reagents will be attracted to regions of negative potential [23]. This will also be of importance in molecular recognition processes, where a drug-receptor interaction may be predicted through an evaluation of electrostatic potential.

Table 2. Valence population (P_v), κ parameter and atomic charges (q) for the $Cr(CO)_6$ molecule after κ-formalism refinement

Atom	P_v (e)	κ	q (e)
Cr	4.122(47)	1.398(14)	+0.878(47)
O(1)	6.415(54)	1.016(5)	-0.414(54)
O(2)	6.462(50)	1.010(5)	-0.462(50)
O(3)	6.452(33)	1.017(4)	-0.451(33)
O(4)	6.653(37)	1.001(3)	-0.653(37)
C(1)	3.830(65)	1.075(10)	+0.170(65)
C(2)	3.424(61)	1.124(11)	+0.576(61)
C(3)	3.824(40)	1.079(8)	+0.176(40)
C(4)	3.445(45)	1.128(9)	+0.554(45)
		Total charge*:	+0.000

*in the asymmetric unit

The next step in the refinement is to account for the valence shell deformations, *i.e.,* the actual non-spherical contribution to the electron density. One of the methods used for this purpose is known as the *multipolar model*, which consists of a diversity of formalisms proposed throughout the years (*e.g.* [25-27]). One of the most used interpretation and the one adopted here is the Hansen-Coppens formalism [27], described by Eq. (4). Comparing this equation to Eq. (3), one can see that a third term was added. This term accounts for the valence deformation, that means truly asphericity, where R_l are radial functions, $P_{lm\pm}$ are multipole populations and $d_{lm\pm}$ are normalized spherical harmonics.

$$\rho_{atom}(\boldsymbol{r}) = \rho_{core}(\boldsymbol{r}) + P_v\kappa^3\rho_{valence}(\kappa r) + \sum_{l=0}^{l_{max}} \kappa'^3 R_l(\kappa' r) \sum_{m=0}^{l} P_{lm\pm} d_{lm\pm}(\theta,\phi) \quad (4)$$

The Hansen-Coppens formalism has the advantage of using a local coordinate system to define the set of atomic functions. This coordinate system is independent of the unit cell axes and enables the transferability of multipolar parameters from one atom in a simple molecule to an equivalent atom in a more complex structure. This approach is particularly useful in the study of macromolecules, such as polypeptides, proteins or other biomolecules, which are too large for theoretical calculations (hundreds of atoms), and usually do not yield good quality single-crystals for a high-resolution diffraction data collection. For these matters, there are some available databanks, from which it is possible

to extract the pseudoatomic properties and apply it to atoms in a similar environment but in a different crystal (*e.g.* [28,29]).

The multipole refinement consists on refining the multipole populations ($P_{lm\pm}$) and their respective κ' parameters, which are the expansion/contraction coefficients associated with the aspherical deformation density (unlike the κ parameter, which is associated to the spherical valence density). However, the refinement of κ' can sometimes lead to convergence problems, which are usually avoided by the use of a Kappa Restricted Multipole Model (KRMM), which consists of fixing the κ' parameters to values obtained through the refinement of theoretical structure factors (lacking experimental errors) [30]. Furthermore, depending on the local symmetry around an atom, some functions either vanish or have a $P_{lm\pm}$ value close to zero [31]. In such cases, the corresponding population should be fixed to zero, decreasing the number of parameters refined and avoiding instabilities in the refinement.

The multipole expansion level is dependent on the type of atoms involved. Usually, H atoms should not be refined over the quadrupole level ($l = 2$), elements from the second period are typically refined up to the octupole level ($l = 3$), and elements from the third period onwards can be refined up to the hexadecapole level ($l = 4$). For instance, transition metals can be extended up to the hexadecapole level, while C and O atoms are usually refined up to the octupole level, but depending on data quality, they can also be refined up to the hexadecapole level. It is important to note though, that despite the fact that multipolar functions present shapes resembling orbitals, the X-ray diffraction experiment can only retrieve information regarding electron density distribution (which is a quantum-mechanical observable), not atomic nor molecular orbitals, which are mathematical concepts (not observables) [32].

The results for the multipole refinement of $Cr(CO)_6$ shown here will be evaluated after the refinement of each multipole expansion level, in order to visualize the model improvements. However, the refinement of multipoles could be done in one single step. To evaluate the improvements, deformation maps (one of the model quality indicators) are used in addition to residual densities. These maps are obtained through the difference between the density from the multipolar expansion and the IAM, Eq. (5), in reciprocal space, just like residual density functions, and for good quality data and adequate model fitting, these maps should show density only in regions of chemical bonds and lone pairs.

$$\Delta\rho(\boldsymbol{r}) = \rho_{multi}(\boldsymbol{r}) - \rho_{IAM}(\boldsymbol{r}) \quad (5)$$

Deformation density maps may also inform on the presence of intermolecular interactions through the presence of charge accumulation between atoms. As it happens for hydrogen bonds, for example, the extent of the deformation in the bond direction is inversely related to the hydrogen bond distance, *i.e.*, strong hydrogen bonds (short distance) present a larger electron deformation and weaker hydrogen bonds (longer distances) present smaller deformations [33]. However, the X-ray diffraction experiment is not capable of precisely localizing the position of hydrogen atoms. To remediate this, a combination of X-ray and neutron diffraction can be performed, or hydrogen atoms can be fixed at positions determined by a neutron diffraction experiment.

For the molecule under study, it was assumed that atoms Cr, C(1), C(2), O(1) and O(2) present local symmetry *m*, consistent with what would be expected from their crystallographic position in the unit cell, while the remaining atoms were assumed to have no symmetry (*i.e.* general positions). The choice of a local coordinate system can be done according to the local symmetry by the use of the Table 4 from ref. [31], also available in the XD2016 manual. The atoms with symmetry *m*, for instance, will present *z*-axis perpendicular to the mirror plane. According to the symmetry and the presence of atoms in special positions, some constraints are imposed on the refined parameters. For example, in the case of the atoms here studied presenting symmetry *m*, the positional parameter *y* does not need to be refined, and thermal parameters U_{21} and U_{23}, along with the multipole functions D0, Q1±, O0, O2±, H1± and H3± can all be fixed at zero. Furthermore, in some cases, it is possible to assume chemical constraints, applied to atoms with similar neighborhoods, causing just one of them to be refined, while the other(s) become chemically equivalent. They will present the same parameter values, lowering the overall number of parameters to be refined. After the refinement of the dipole functions for every atom, it is already possible to see a small modification on the deformation map in comparison to that from the spherical model, especially around the O atoms, Fig. 4, although the improvement is not very significant yet.

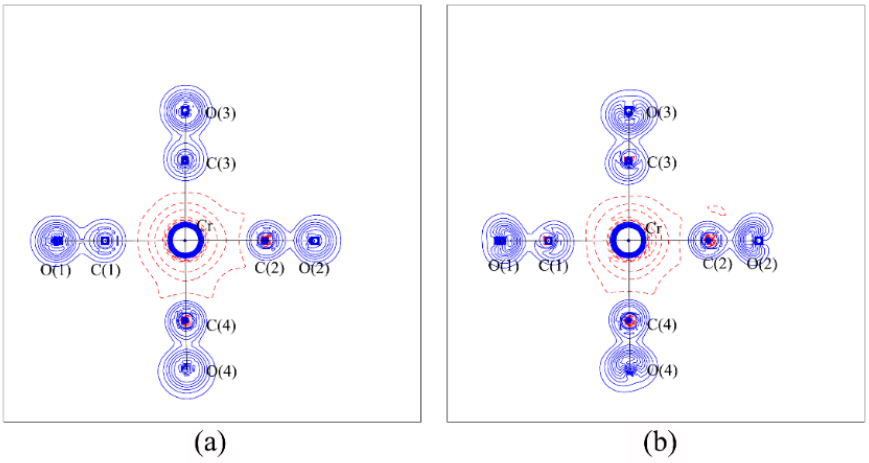

Figure 4. Deformation density maps after (a) the κ-formalism refinement and (b) the dipole refinement.

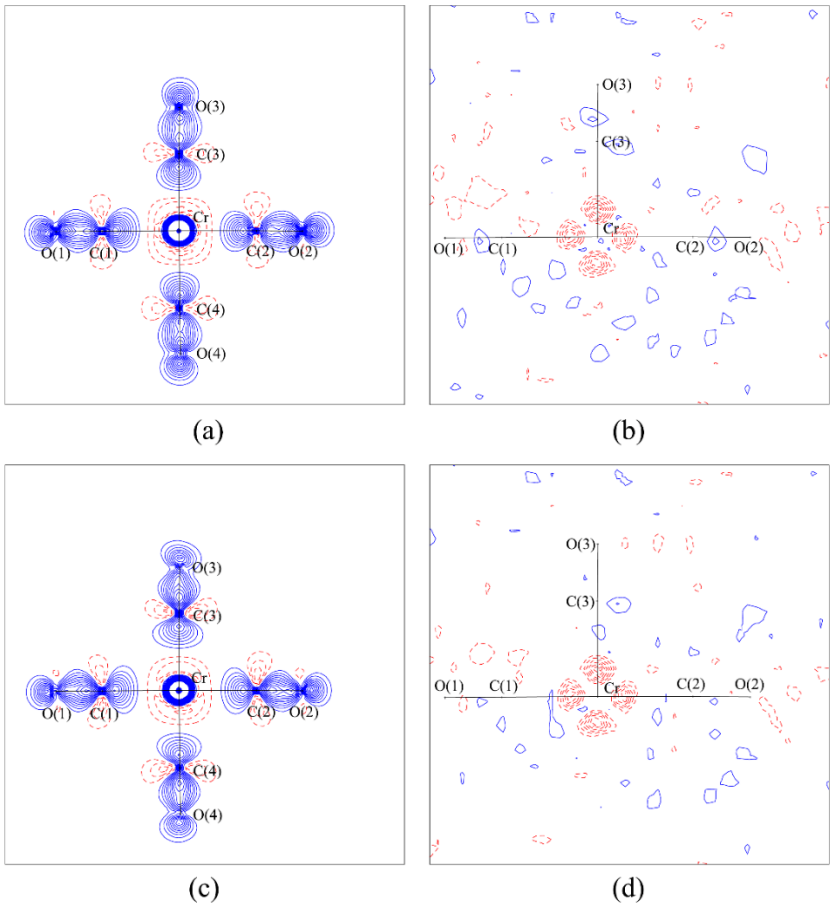

Figure 5. (a) Deformation and (b) residual density maps obtained after the quadrupole refinement, and (c) deformation and (d) residual density maps obtained after the octupole refinement.

The next multipoles to be refined are the quadrupole and the octupole sets respectively. The deformation density and residual density maps obtained after the quadrupole and octupole refinements are depicted in Fig. 5. It is possible to see that after

the quadrupole refinement, the deformation density map is already informative regarding C and O atoms, Fig. 5(a), but the residual density map still shows some electron density residue on the C≡O bonds, Fig. 5(b), indicating that the model is still not sufficiently adequate. The octupole refinement is then carried out, and it is now possible to see that the C and O atoms have only random noise in the residual map, Fig. 5(d), but the transition metal, on the other hand, still has some significant residual density left.

Since transition metals present *d*-orbitals, it is appropriate to refine the hexadecapolar functions for these atoms. Transition metals have some particularities in their refinement due to the diffuse nature of the *n*s electrons, which hinders the association of these electrons as belonging to the metal or to the ligand [34]. However, despite the inherent difficulties in treating these elements, the current technological advancements have allowed higher accuracy in the description of their properties.

After the hexadecapole refinement for the Cr atom, the final residual density map is featureless, indicating good agreement between observed and calculated structure factors, Fig. 6(b). The deformation density map presents charge concentration in regions related to chemical bond and oxygen lone pairs, while the transition metal presents charge depletion in the direction of the ligands and charge concentration in the direction bisecting the ligands, as it is expected from crystal field theory, Fig. 6(a).

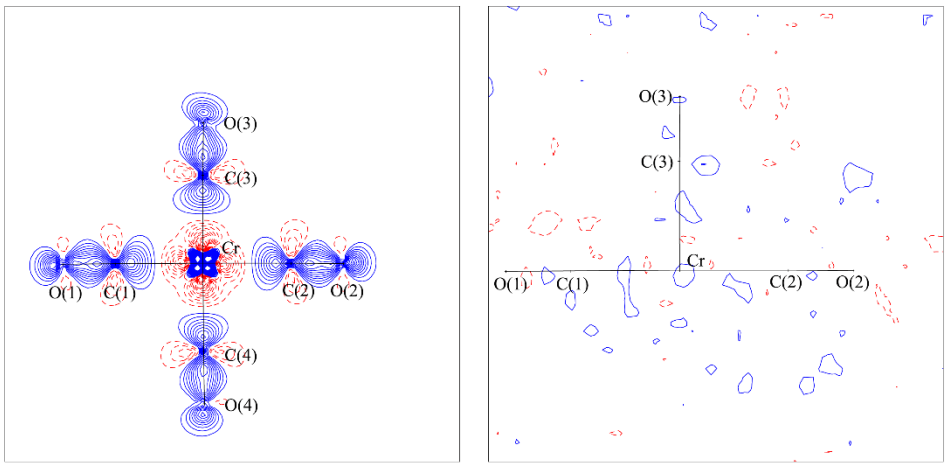

Figure 6. (a) Deformation and (b) residual density maps obtained after the hexadecapole refinement.

The last adjustment to be made is related to the κ' parameter. The refinement of this parameter is not always possible, so they are usually fixed to values extracted from the

literature, as it is the case for the molecule under study. The κ' values used here were obtained from the refined values for $Cr(CO)_6$ in ref. [16]. The final maps calculated after fixing the κ' parameter values are shown in Fig. 7. Even though there is no visible modification to the deformation density map in relation to that from Fig. 6(a), the residual density map shows slightly less residues, indicating that the model has improved, at least a little.

In some cases, the presence of remaining residual density around an atom, usually in a pattern of alternating positive and negative residual density, might indicate the need to consider the anharmonic motion in the analysis. Along with the residual density pattern, the presence of anharmonic motion can also be evaluated through the probability density function, which will present deviations from a Gaussian distribution if anharmonic motion is present [35]. The refinement of anharmonic thermal parameters is done through the Gram-Charlier coefficients, and the suitability of the data to this type of refinement can be evaluated through Kuhs' rule [36], which will estimate the minimum required resolution (Q_n) for the refinement. Kuhs' rule is given by $Q_n = 2n^{1/2}(2\pi)^{-1/2}(2\,ln2)^{1/2} < u^2 >^{-1/2}$, where n = 3 or 4 (third- or fourth-order Gram-Charlier coefficients). However, Herbst-Irmer *et al*. [35] have demonstrated that Kuhs' rule seems to be more appropriate for lighter atoms, such as carbon, as opposed to heavier atoms, such as phosphorus.

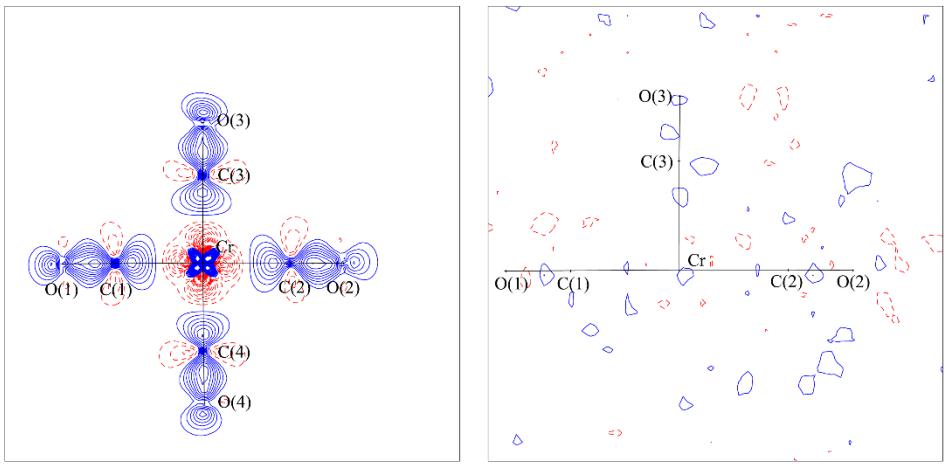

Figure 7. (a) Deformation and (b) residual density maps for the final model.

Along with the maps, other indicators of model quality could be evaluated [17], such as: statistical parameters, probability distribution and scale factor *vs*. resolution plots, and the Hirshfeld rigid bond test. These indicators will be briefly discussed below.

4. Quality of the refined model

The comparison of statistical parameters for each refinement stage is found in Table 3, where one can see great improvement in model adequacy (lowering of the values). The probability distribution and scale factor *vs.* resolution plots for the final model can be seen in Fig. 8, where they are compared to those obtained after the IAM refinement. The probability distribution plot for the final model has a maximum residual density of 0.2 and minimum of -0.2 eÅ^{-3}, a much better result than that obtained for the IAM refinement, 0.8 and -0.8 eÅ^{-3}, Fig. 8(a). The scale factor *vs*. resolution plot evaluates whether the scale factor $[k = \sum(F_{obs}^2)/\sum(F_{calc}^2)]$ is approximately constant throughout the resolution shells or vary substantially. The plot obtained for the final refinement also demonstrates the improvement of the model, with maximum excursion of approximately 2%, while that for the IAM is close to 5%, Figure 8(b). Finally, a comparison of the differences of mean-squares displacements amplitudes (DMSDA) is shown in Table 4. According to the Hirshfeld rigid bond test [37], these values should not be higher than 0.001 Å^2, this would indicate an optimal deconvolution between deformation density related to bonding from an instantly non-spherical contribution due to thermal vibration. The values were already acceptable in the conventional refinement (a result expected from the unusually low temperature in which the data was acquired), but the multipole refinement improves these results even more.

Table 3. Statistical parameters for the different levels of refinement

Level	R(F)	R(F^2)	wR(F)	wR(F^2)	S	no. of parameters refined
IAM	0.0189	0.0255	0.0298	0.0526	5.1784	67
κ-formalism	0.0191	0.0257	0.0192	0.0379	4.3224	84
Dipole	0.0190	0.0251	0.0186	0.0366	4.2020	106
Quadrupole	0.0133	0.0162	0.0109	0.0208	2.4640	141
Octupole	0.0129	0.0150	0.101	0.0193	2.3153	189
Hexadecapole	0.0110	0.0132	0.0086	0.0161	1.9689	194
κ’	0.0110	0.0130	0.0084	0.0156	1.9212	194

$R(F) = \sum|F_{obs} - kF_{calc}|/\sum|F_{obs}|$; $wR(F) = [\sum w(F_{obs} - kF_{calc})^2/\sum w|F_{obs}^2|]^{1/2}$;

$S = [\sum w(\Delta f)^2/(N_{ref} - N_{var})]^{1/2}$, where $\Delta f = F_{obs} - kF_{calc}$, N_{ref} = number of observations, N_{var} = number of independent variables in the refinement. k denotes a scaling factor.

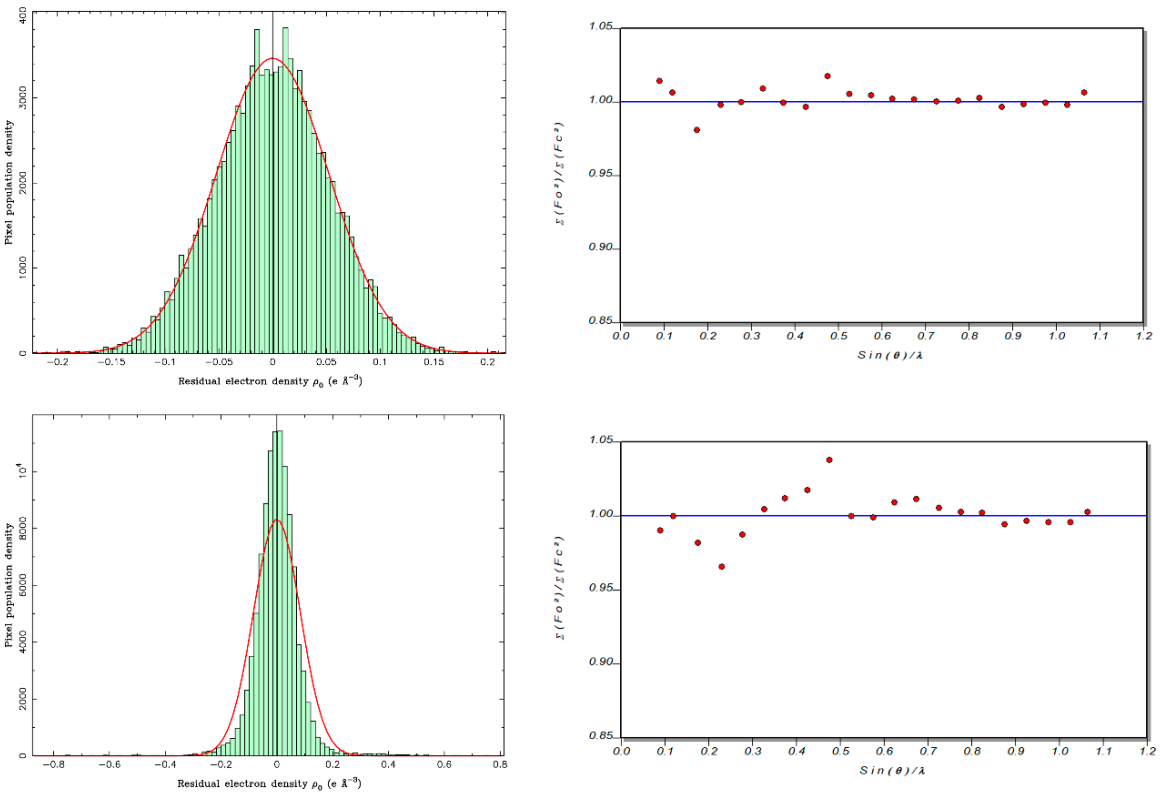

Figure 8. (a) Probability distribution and (b) scale factor *vs*. resolution plots for the final model (upper) and the IAM refinement (bottom).

Table 4. Differences of Mean-Squares Displacement Amplitudes for the different levels of refinement (Å^2)

	C(1)–O(1)	C(2)–O(2)	C(3)–O(3)	C(4)–O(4)
IAM	0.0005	0.0006	0.0003	0.0005
κ-formalism	0.0005	0.0005	0.0004	0.0005
Dipole	0.0004	0.0004	0.0003	0.0005
Quadrupole	0.0002	0.0003	-0.0002	0.0002
Octupole	0.0000	0.0001	-0.0004	0.0000
Hexadecapole	0.0001	0.0002	-0.0003	0.0001
κ’	0.0001	0.0002	0.0001	0.0001

5. Topological Analysis

The multipole refinement allows for the calculation of properties related to the electron density. For instance, a topological analysis may be performed, which is based on Bader’s Quantum Theory of Atoms in Molecules (QTAIM) [8] and allows for the identification of critical points in the electron density gradient. The critical points are

classified according to a pair (ω,σ), where ω is related to the rank of the 3 × 3 Hessian matrix and σ relates the algebraic summation of the signs of the three principal curvatures of ρ. In this manner, the critical point (3,-3) indicates a local maximum in the electron density, and it is usually associated to a nucleus, while the (3,+3) critical point, known as a cage critical point, is related to a local minimum. The (3,-1) critical point is known as a bond critical point, while the (3,+1) is regarded as a ring critical point, both being saddle points on the density. The gradient vector field for the electron density is shown in Fig. 9, where the bond critical points are represented as blue dots. From each bond critical point, two trajectories of maximum electron density leave and connect two nuclei, these trajectories are known as a bond path, which is usually associated to the presence of a chemical bond, indicated as black lines in Fig. 9. QTAIM partitions the molecule electron density into atomic basins, delimited by a zero-flux surface, in a manner as all electrons inside the surface are bound to the corresponding nucleus inside the same surface. These surfaces are represented by the thicker brown lines in Fig. 9. The quantitative information related to the topological descriptors is available in Table 5. It is interesting to notice the higher electron density at the bond critical point for the triple bonds C≡O, indicating their strengths. The descriptor ε (ellipticity) is a measure of the π character of the bond, being zero for a cylindrically symmetric bond, such as single or triple bonds. The majority of the ε values obtained for compound $Cr(CO)_6$ are close to zero, as it would be expected considering the nature of the covalent bonds present in the compound. Interestingly, most of the higher ellipticity values are associated to metal-carbonyl bonds, thus indicating some π character, as one would expect from metal back donation to the ligand. The Laplacian of the density, $\nabla^2\rho(\boldsymbol{r}_{BCP})$, at a particular bond critical point, can be seen as the sum of the three principal curvatures of the function at that point. It informs on charge concentration or depletion. As shown in Table 5, it is usually positive for closed shell bonds and negative for the more covalent ones, but its quantitative interpretation must be made with great care.

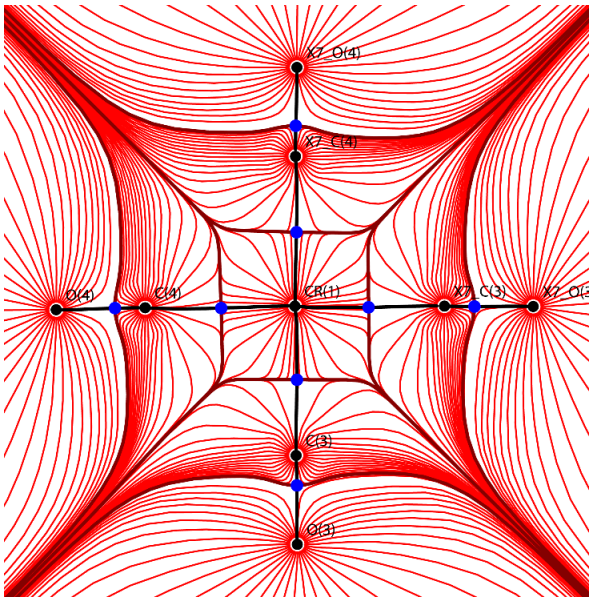

Figure 9. Trajectories of the gradient vector field for $Cr(CO)_6$. Red lines represent trajectories, brown lines delimit the zero-flux surfaces, black lines are bond paths, black dots are associated with nuclei and blue dots with bond critical points.

Table 5. Some topological descriptors of the electron density

	d (Å)	$\rho(\boldsymbol{r}_{BCP})$ (eÅ^{-3})	$\nabla^2\rho(\boldsymbol{r}_{BCP})$ (eÅ^{-5})	ε
Cr–C(1)	1.9124	0.714(4)	12.833(7)	0.05
Cr–C(2)	1.9176	0.721(4)	12.316(7)	0.08
Cr–C(3)	1.9152	0.692(4)	13.323(7)	0.02
Cr–C(4)	1.9205	0.666(5)	13.036(7)	0.05
O(1)–C(1)	1.1427	3.411(16)	-12.856(103)	0.01
O(2)–C(2)	1.1427	3.305(15)	2.424(87)	0.04
O(3)–C(3)	1.1413	3.315(15)	-0.734(107)	0.03
O(4)–C(4)	1.1405	3.335(20)	-5.674(137)	0.06

6. Recent Applications of Charge Density Analysis

The fact that the properties of a material are highly dependent on the nature and strength of chemical bonds, intermolecular interactions, and on the overall arrangement of atoms, makes charge density studies a valuable tool for understanding and predicting such properties. Nowadays, one can find in the literature many useful applications for charge

density studies, either experimentally or theoretically determined (for example by means of first-principle quantum mechanics or dynamics).

One of the most appealing applications concern crystal engineering, that is related to efficiently arranging molecules in the unit cell in a way as to optimize a given materials property. In this regard, intermolecular interactions are fundamental as the source of crystal packing in molecular materials. Among the weak interactions, the hydrogen bond is special because of its varied nature, ranging from partially covalent to weakly electrostatic. It can be highly directional, if contains a large covalent component, but much less so if it is based on electrostatic forces. The energy of hydrogen bonds spans the range from a few kJ/mol to approximately 100 kJ/mol. Despite their diversity, a unifying approach that includes all the hydrogen bonds is highly desirable, although still lacking. Numerous works have collected very accurate, low-temperature, high resolution X-ray diffraction data on hydrogen-bonded organic co-crystals in order to quantitatively characterize the nature and energetics of many hydrogen bonds through QTAIM analysis of the electron density distribution, see [33] for an example. On the one hand, such studies show that many features of the electron density in the hydrogen bond region can be accurately retrieved using X-ray diffraction data alone, at variance with the past, when neutron diffraction was widely used to fix accurate atomic positions. On the other hand, by spanning a hydrogen bond length from *c.a.* 1.4 to 2.5 Å, it can be confirmed that a unified hydrogen bond theory based on accurate electron density indicators is indeed possible because these indices usually vary smoothly with the hydrogen bond length. This is of course remarkably relevant to engineer molecular crystals. In addition, the development of the method known as the Hirshfeld atom refinement (HAR) allows the estimation of H-atom positions and ADPs very close to those determined by neutron diffraction [38]. This method uses the Hirshfeld stockholder partitioning scheme [39] and *ab initio* calculations to obtain scattering factors and thus, the atomic coordinates and ADPs.

To gain more information on the chemical bonding from electron density analysis other than that already available from the traditional Hansen-Copens models, the so-called X-ray constrained wave function methods have emerged. They are Slater determinants, which minimizes a functional given by the corresponding energy and a statistical agreement with the experimental X-ray diffraction data [40]. It is additionally possible to combine the X-ray constrained wave function approach with the typical interpretability of

the pseudoatom models by using molecular orbitals strictly localized on atoms, bonds or functional groups [41]. Capabilities and limitations of this new technique have been accessed using very high-quality X-ray diffraction data aiming at studying the efficiency of the method in molecular materials and testing the transferability of the localized orbitals to larger systems. The most important outcome could be related to devising new strategies for refining crystallographic structures and electron densities of macromolecules, such as polymers or proteins.

This synergy between experiment and theory has been fruitful in many ways. One of the properties widely studied through charge density is the magnetic susceptibility of materials, especially those presenting transition metals, since the evaluation of *d*-orbital occupations, along with information on intra- and intermolecular interactions, may be informative on preferred magnetic directions in the crystal. Some studies focusing on this correlation can be found in references [42-45]. Other interesting application is related to superconducting materials. Although less frequent in the literature due to difficulties in obtaining high quality crystals of such materials, the availability of synchrotron sources has allowed charge density studies in some of these materials [46]. The charge density analyses of quasi one-dimensional Sc_3TC_4 (T = Fe, Co and Ni), for instance, has allowed the observation that the out-of-plane distortion modes present in the Co congeners of the series and absent in the Fe and Ni ones, along with an increase in the density of states, could be taken as prerequisites for superconductivity properties in the Co carbide [47,48].

7. Concluding Remarks

Much knowledge regarding chemical bonding and structure-property relationships has been acquired over the last decades thanks to the development of the aspherical atom refinement and the topological analysis. Charge density analyses have contributed greatly to the field of materials science as it allows a deeper understanding of physical properties and their causes. In order to perform such studies, one must obtain high-resolution X-ray data measured at low temperatures, techniques that are becoming more accessible and reliable with the increasing technological advancements.

Acknowledgments

Financial support by CAPES (88882.348238/2019-01).

References

[1] C. R. GROOM, I. J. BRUNO, M. P. LIGHTFOOT, S. C. WARD. *Acta Cryst.* B**72**, 171-179 (2016).

[2] P. COPPENS *Acta Cryst.* A54, 779-788 (1998).

[3] P. COPPENS *J. Chem. Educ.* **61**, 761-765 (1984).

[4] F. K. LARSEN. *Acta Cryst*. B**51**, 468-482 (1995).

[5] V. V. ZHUROV, E. A. ZHUROVA, A. I. STASH, A. A. PINKERTON. *Acta Cryst.* A**67**, 160-173 (2011).

[6] S. MONDAL, S. J. PRATHAPA, S. van SMAALEN. *Acta Cryst.* A**68**, 568-581 (2012).

[7] M. R. V. JØRGENSEN, V. R. HATHWAR, N. BINDZUS, N. WAHLBERG, Y.-S. CHEN, J. OVERGAARD, B. B. IVERSEN. *IUCrJ* **1**, 267-280 (2014).

[8] BADER, R. F. W. Atoms in Molecules: a Quantum Theory. Clarendon Press, 1990.

[9] A. VOLKOV, P. MACCHI. Unpublished work.

[10] S. PILLET, M. SOUHASSOU, C. MATHONIÈRE, C. LECOMTE. *J. Am. Chem. Soc.* **126**, 1219-1228 (2004).

[11] A. CHOUAIH, F. HAMZAOUI, G. VERGOTEN. *J. Mol. Struct.* **738**, 33-38 (2005).

[12] N. CASATI, A. GENONI, B. MEYER, A. KRAWCZUK, P. MACCHI. *Acta Cryst.* B**73**, 584-597 (2017).

[13] P. M. DOMINIAK, A. VOLVKOV, X. LI, M. MESSERSCHMIDT, P. COPPENS. *J. Chem. Theory Comput.* **3**, 232-247 (2007).

[14] B. N. FIGGIS, A. N. SOBOLEV. *Acta Cryst.* E**60**, i93-i94 (2004).

[15] B. REES, A MITSCHLER. *J. Am. Chem. Soc.* **98**, 7918-7924 (1976).

[16] L. J. FARRUGIA, C. EVANS. *J. Phys. Chem. A* **109**, 8834-8848 (2005).

[17] V. V. ZHUROV, E. A. ZHUROVA, A. A. PINKERTON. *J. Appl. Cryst.* **41**, 340-349 (2008).

[18] G. M. SHELDRICK. SHELXS-86 - A program for automatic solution of crystal structures. *Acta. Cryst*. A**46**, 467-473 (1990).

[19] G.M. SHELDRICK. Crystal structure refinement with SHELXL, *Acta Cryst*., C**71**, 3-8 (2015).

[20] VOLKOV, A., MACCHI, P., FARRUGIA, L. J., GATTI, C., MALLINSON, P., RICHTER, T., KORITSANSZKY, T. (2016). XD2016 – a computer program for

multipole refinement, topological analysis of charge densities and evaluation of intermolecular interaction energies from experimental or theoretical structure factors.

[21] GIACOVAZZO, C., MONACO, H. L., VITERBO, D., SCORDARI, F., GILLI, G., ZANOTTI, G., CATTI, M. Fundamentals of Crystallography. New York: Oxford University Press, 1992.

[22] K. MEINDL, J. HENN. *Acta Cryst.* A**64**, 404-418 (2008).

[23] COPPENS, P. X-Ray Charge Densities and Chemical Bonding, Oxford University Press, 1997.

[24] A. VOLKOV, Y. A. ABRAMOV, P. COPPENS. *Acta Cryst.* A**57**, 272-282 (2001).

[25] F. L. HIRSHFELD. *Acta Cryst.* B**27**, 769-781 (1971).

[26] R. F. STEWART. *J. Chem. Phys.* **58**, 1668-1676 (1976).

[27] N. K. HANSEN, P. COPPENS. *Acta Cryst.* A**34**, 909-921 (1978).

[28] A. VOLKOV, X. LI, T. KORITSANSZKY, P. COPPENS. *J. Phys. Chem. A* **108**, 4283-4300 (2004).

[29] P. M. DOMINIAK, A. VOLKOV, X. LI, M. MESSERSCHMIDT, P. COPPENS. *J. Chem. Theory Comput.* **3**, 232-247 (2007).

[30] Y. A. ABRAMOV, A. V. VOLKOV, P. COPPENS. *Chem. Phys. Lett.* **311**, 81-86 (1999).

[31] K. KURKI-SUONIO. *Isr. J. Chem.* **16**, 115-123 (1977).

[32] T. S. KORITSANSZKY, P. COPPENS. *Chem. Rev.* **101**, 1583-1627 (2001).

[33] L. H. R. DOS SANTOS, B. L. RODRIGUES, Y. M. IDEMORI, N. G. FERNANDES. *J. Mol. Struct.* **1014**, 102-109 (2012).

[34] P. COPPENS. *Coord. Chem. Rev.* **65**, 285-307 (1985).

[35] R. HERBST-IRMER, J. HENN, J. J. HOLSTEIN, C. B. HÜBSCHLE, B. DITTRICH, D. STERN, D. KRATZERT, D. STALKE. *J. Phys. Chem. A* **117**, 633-641 (2013).

[36] W. F. KUHS. *Acta Cryst.* A**48**, 80-98 (1992).

[37] F. L. HIRSHFELD. *Acta Cryst.* A**32**, 239-244 (1976).

[38] D. JAYATILAKA, B. DITTRICH. *Acta Cryst.* A**64**, 383-393 (2008).

[39] F. L. HIRSHFELD. *Theoret. Chim. Acta (Berl.)* **44**, 129-138 (1977).

[40] A. GENONI. *J. Phys. Chem. Lett.* **4**, 1093-1099 (2013).

[41] L. H. R. DOS SANTOS, A. GENONI, P. MACCHI. *Acta Cryst.* A**70**, 532-551 (2014).

[42] R. D. POULSEN, A. BENTIEN, M. CHEVALIER, B. B. IVERSEN. *J. Am. Chem. Soc.* **127**, 9156-9166 (2005).

[43] H. F. CLAUSEN, J. OVERGAARD, Y. S. CHEN, B. B. IVERSEN. *J. Am. Chem. Soc.* **130**, 7988-7996 (2008).

[44] L. H. R. DOS SANTOS, A. LANZA, A. M. BARTON, J. BRAMBLEBY, W. J. A. BLACKMORE, P. A. GODDARD, F. XIAO, R. C. WILLIAMS, T. LANCASTER, F. L. PRATT, S. J. BLUNDELL, J. SINGLETON, J. L. MANSON, P. MACCHI. *J. Am. Chem. Soc.* **138**, 2280-2291 (2016).

[45] E. DAMGAARD-MØLLER, L. KRAUSE, H. LASSEN, L. A. MALASPINA, S. GRABOWSKY, H. BAMBERGER, J. McGUIRE, H. N. MIRAS, S. SPROULES, J. OVERGAARD. *Inorg. Chem.* **59**, 13190-13200 (2020).

[46] T. LIPPMANN, P. BLAHA, N. H. ANDERSEN, H. F. POULSEN, T. WOLF, J. R. SCHNEIDER, K.-H. SCHWARZ. *Acta Cryst.* A**59**, 437-451 (2003).

[47] B. ROHRMOSER, G. EICKERLING, M. PRESNITZ, W. SCHERER, V. EYERT, R.-D. HOFFMANN, U. C. RODEWALD, C. VOGT, R. PÖTTGEN. *J. Am. Chem. Soc.* **129**, 9356-9365 (2007).

[48] W. SCHERER, C. HAUF, M. PRESNITZ, E.-W. SCHEIDT, G. EICKERLING, V. EYERT, R.-D. HOFFMANN, U. C. RODEWALD, A. HAMMERSCHMIDT, C. VOGT, R. PÖTTGEN. *Angew. Chem. Int. Ed.* **49**, 1578-1582 (2010).